Fast Automatic Path Proposal Computation for Hepatic Needle Placement

Christian Schumann[a], Jennifer Bieberstein[a], Christoph Trumm[b], Diethard Schmidt[c], Philipp Bruners[d], Matthias Niethammer[e], Ralf T. Hoffmann[b], Andreas H. Mahnken[d], Philippe L. Pereira[f] and Heinz-Otto Peitgen[a]

[a]Fraunhofer MEVIS - Institute for Medical Image Computing, Bremen, Germany;
[b]Ludwig-Maximilians-University of Munich, Dept. of Clinical Radiology, Munich, Germany;
[c]University Hospital Tübingen, Dept. of Radiology, Tübingen, Germany;
[d]RWTH Aachen University Hospital, Dept. of Diagnostic Radiology, Aachen, Germany;
[e]Siemens AG Healthcare Sector, Forchheim, Germany;
[f]SLK Clinic, Heilbronn, Germany

ABSTRACT

Percutaneous image-guided interventions, such as radiofrequency ablation (RFA), biopsy, seed implantation, and several types of drainage, employ needle shaped instruments which have to be inserted into the patient's body. Precise planning of needle placement is a key to a successful intervention. The planning of the access path has to be carried out with respect to a variety of criteria for all possible trajectories to the selected target. Since the planning is performed in 2D slices, it demands considerable experience and constitutes a significant mental task. To support the process of finding a suitable path for hepatic interventions, we propose a fast automatic method that computes a list of path proposals for a given target point inside the liver with respect to multiple criteria that affect safety and practicability. Prerequisites include segmentation masks of the liver, of all relevant risk structures and, depending on the kind of procedure, of the tumor. The path proposals are computed based on a weighted combination of cylindrical projections. Each projection represents one path criterion and is generated using the graphics hardware of the workstation. The list of path proposals is generated in less than one second. Hence, updates of the proposals upon changes of the target point and other relevant input parameters can be carried out interactively. The results of a preliminary evaluation indicate that the proposed paths are comparable to those chosen by experienced radiologists and therefore are suited to support planning in the clinical environment. Our implementation focuses on RFA and biopsy in the liver but may be adapted to other types of interventions.

Keywords: minimally invasive intervention, radiofrequency ablation, therapy planning, access path planning

1. INTRODUCTION

Minimally invasive image-guided interventions have been an important part of diagnostic and therapeutic radiology for 30 years. In the field of diagnosis, image-guided percutaneous biopsy is a widely established and safe method for the differentiation of malignant and benign tumors[1]. Therapeutic applications include drainage, seed implantation for brachytherapy, musculo-skeletal interventions, and, especially in the field of interventional oncology, thermal ablation procedures such as radiofrequency ablation (RFA), laser ablation, and microwave ablation for the destruction of tumors. In particular, percutaneous RFA has become an established treatment option for early hepatocellular carcinoma and for metastatic liver tumors not suited for surgical resections. This minimally invasive therapy induces a high-frequency alternating current into the tumor tissue which is destroyed due to the resulting heat. Major advantages of RFA are minimal trauma for the patient, low complication rates, and good overall survival rates[2]. The alternating current is induced by means of a radiofrequency (RF) applicator which resembles a needle. Several applicator types may extend active tips of differing size and configuration to

Further author information: (Send correspondence to C. Schumann)
C. Schumann: E-mail: christian.schumann@mevis.fraunhofer.de, Telephone: +49 421 218 7722

achieve a coagulation area with a larger size and a better suited shape. However, these tips are not deployed until the applicator placement has been finished. Hence, RFA, using any of those applicator types, as well as biopsy, seed implantation, and several types of drainage face similar challenges during planning of the intervention: A linear path to the target has to be found that fulfills multiple criteria. These include several geometric properties that affect the safety and practicability of the path. Assessing all these criteria for all possible trajectories by examining only 2D slices of the CT or MR planning scan is a demanding task and requires considerable experience. Therefore, the process of planning hepatic interventions and interventions in general can benefit from computer assistance.

We propose a method that automatically computes a list of suitable path proposals for a given target point inside the liver to support the planning process for RFA and biopsy. Prerequisites include segmentation masks of the liver, of the skin, of all relevant risk structures, and of the tumor in the case of tumor ablation therapies. The method uses techniques from the fields of computer graphics and image processing and works directly on segmentation masks instead of polygonized surfaces. The utilization of the graphics hardware of the workstation effectuates very low computation times. The list of access path proposals is generated in less than one second. Hence, the target point can be changed interactively.

2. RELATED WORK

Several approaches to support path determination for RFA and similar techniques have been proposed in recent years. Almost all methods focus on the optimization of the coverage of the tumor by the expected ablation area. For that purpose, these methods either approximate the ablation area by an ellipsoid or perform an exact simulation of the ablation area.

The approximation of the ablation area by ellipsoids for the purpose of coverage optimization was pioneered by Butz et al.,[3] who use Powell's optimization algorithm[4] to automatically improve the placement of a manually positioned applicator for cryo ablation or RFA. A comparable approach was presented by Villard et al.[5] They compare Powell's method with downhill simplex optimization and choose the latter for their approach. Avoidance of vital structure penetration is considered as an additional criterion. However, this constraint is too strong and sometimes restricts the optimization process to a zone that is surrounded by anatomical strutures. Zhang et al.[6] use Powell's method and simulated annealing to cover the tumor with multiple ablations. As recently published, Mundeleer et al.[7] use a downhill simplex optimization scheme for the coverage of the tumor by multiple spherical ablation zones. Trovato et al.[8] propose a very fast method that utilizes fixed constellations of elliptical ablation areas to solve the coverage problem for a given skin entry point.

The exact prediction of the ablation area, including the cooling effects of surrounding blood vessels using finite elements, forms the basis of the method of Altrogge et al.[9] The optimization of the applicator placement is carried out using a gradient descent method. No additional constraints are taken into account, and the computational times are in the range of minutes. Chen et al.[10] combine the finite elements approach with a new optimization strategy that exploits the fact that over small variations of applicator parameters, the ablation shape changes slowly. The applicability of the method to clinical data is not subject of that publication, however.

To the best of our knowledge only the method of Baegert et al.[11] focuses on the incorporation of multiple clinically relevant criteria. It utilizes a downhill simplex based optimization method for the generation of access path proposals with regard to multiple criteria. The duration as well as the quality of the results strongly depend on the resolution of the polygonal representations, which are used as input[12]. The mean duration for the path generation is approximately 30 seconds. However, this does not include the polygonization of the relevant anatomical structures.

3. ANALYSIS OF RELEVANT PATH CONSTRAINTS

The suitability of a path for hepatic needle insertion is influenced by a number of criteria, which we denote *path constraints* in the subsequent text. First of all, a path has to be as safe as possible. Therefore, anatomical structures such as vessels, pleural space, and adjacent organs should not be traversed[1]. Trajectories that are far away from risk structures should be preferred to trajectories close to risk structures. Furthermore, the path should include a transhepatic route long enough to realize a tamponade of a hemorrhage along the puncture

channel[1], and, in the case of ablation procedures, to allow for the cauterization of the path and the fixation of the needle. This is important, because it means that in many cases, the shortest path is not optimal (compare path 1 and path 2 in Figure 1(a)). The angle between the path and the liver surface should not be too small in order to prevent gliding on the surface and the resulting rupture. In the case of ablation procedures, the path should result in a good coverage of the tumor volume by the expected ablation volume. An analysis of these constraints for the path determination for RFA in the liver has been conducted by Baegert et al.[11]

Based on discussions with radiological experts, we identified additional criteria that consider the practicability of access paths. For example, the angulation to the transversal plane should be as low as possible, because the implementation of double oblique paths is more complicated than the implementation of paths that are in plane[1]. Furthermore, collisions of the interventional instrument with the CT or MR scanner msut be avoided. Strongly angulated paths from cranial to caudal, for example, would require the radiologist to work inside the gantry, or the patient table would have to be moved out of the gantry. Trajectories from caudal to cranial are less problematic, because the radiologist can work outside the gantry (Figure 1(b)). Similar restrictions apply to the circumference of the patient body. Depending on the clinical setting, the radiologist usually has a fixed position with respect to the patient table. Therefore, trajectories that demand a position of the radiologist on the opposite side of the table should be excluded (Figure 1(c)). The same holds true for trajectories that would require the physician to adopt an uncomfortable posture. Additionally, posterior entry points should be avoided.

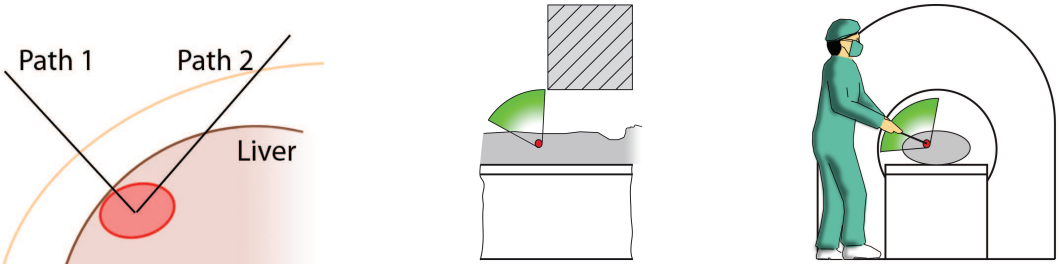

(a) (b) (c)

Figure 1. Different constraints have to be balanced against each other (a): Path 1 is short and can be implemented easily, but does not include enough healthy liver tissue. Path 2 includes enough liver tissue but is more complicated due to the lower liver capsule penetration angle and because it is longer in general. (b): The angulation to the transversal plane is limited due to possible collisions with the gantry *(hatched area)*. (c): The orientation with respect to the body circumference should take the position of the physician into account.

4. METHODS

Our approach is based on the reduction of the path determination problem. We focus on cases in which the target point is clearly defined. For example, in the case of biopsy or radiofrequency ablation of small tumors, the target can easily be defined with one click. Therefore, we consider the trajectory determination for a given target point. For the discretization of the space of all possible trajectories, we use perspective projections. Similar techniques are used in the field of computer graphics to compute shadows[13] or to determine appropriate viewpoints[14,15]. Baegert et al. utilize projections to prevent risk structure penetration in an initial step of their trajectory optimization method[16]. We extend that idea by using projections for all relevant path parameters. The results of the projections are images, which our method directly operates on to extract path proposals. Our algorithm consists of these steps which will be described in detail in the following sections:

1. Generation of constraint maps based on projections
2. Rating of constraint maps
3. Computation of a weighted combination of the rated constraint maps
4. Extraction of suitable trajectories

4.1 Generation of constraint maps

For each of the seven mentioned path constraints, we compute a cylindrical projection with the center at the target point. Because the result of the projection is a 2D image, we refer to it as a *constraint map*. Each of these maps stores the constraint value of one trajectory in each pixel. It projects trajectories of equal longitude to the same column and trajectories of equal latitude to the same row. Both, longitude and latitude lines are equally spaced. The map covers 360° of longitude and 120° of latitude, because trajectories with a latitude less than -60° or more than 60° are not of interest for hepatic needle placement. The image domain corresponds to a two-dimensional spherical coordinate system. We use a resolution of 1 pixel per degree, which results in maps of 360 x 120 pixels.

Two different approaches are used to generate these maps. Most of the constraints have to be computed based on the patient specific data such as segmentation results. We use volume rendering to accomplish that. However, the constraints concerning practicability and tumor coverage can be generated generically. This means we can simply assign values for each trajectory based on the longitude and latitude of the trajectory.

For volume rendering, we use a GPU-based slicing approach. In contrast to CPU raycasting, the projection cannot be customized easily. Instead, we are restricted to using either orthogonal or perspective projections. Therefore, we approximate cylindrical projections by rendering views from multiple stepwise-rotated perspective cameras and stitching them together in the frame buffer (Figure 2(a,b)). However, the use of perspective cameras results in distortions (Figure 2(b)). These can be reduced by using a higher number of cameras (Figure 2(c)). In our implementation we use 45 cameras. Vertical distortions are eliminated by means of a GPU shader program (Figure 2(d)). The following paragraphs outline the generation of the various constraint maps.

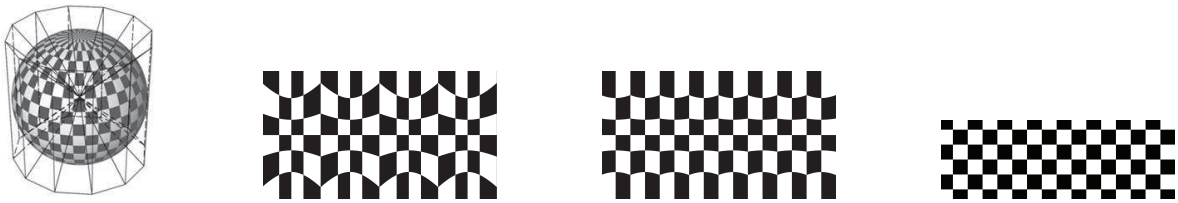

(a) (b) (c) (d)

Figure 2. The cylindrical projection applied to a simple textured sphere. (a): Cylindrical projection is achieved by rendering multiple views (represented by pyramid shaped perspective view frustums) and composing them in the frame buffer. (b): For a small number of cameras (4 cameras), the projection of the textured sphere suffers from severe distortions. (c): Using a higher number of projections greatly reduces the distortions (8 cameras). (d): The use of a high number of cameras and the application of an additional shader eliminates all distortions.

Distance to risk structures: For each trajectory, this map stores the distance of that trajectory to the closest risk structure. To achieve this, we first compute an Euclidean distance transform based on a 3D image that includes the masks of all segmented risk structures. Because this computation is completely independent of the target point, it has to be carried out only once. Hence, it can be implemented as a preprocessing step. To generate the constraint map itself, we compute the cylindrical projection of the *minimum intensity projection* of the distance map (Figure 3(a)). The resulting Euclidean distances are given in millimeters.

Penetration depth: To compute the penetration depth for all possible trajectories, we render the patient skin segmentation mask and extract the z-buffer. The resulting map stores the distance between skin entry point and the target point in millimeters for each trajectory (Figure 3(b)).

Portion of healthy liver tissue: We use the same approach that was used for the previous constraint. This time we render the z-buffer of the liver mask. Since we are interested in the healthy liver tissue only, we subtract the z-buffer of the projected tumor mask.

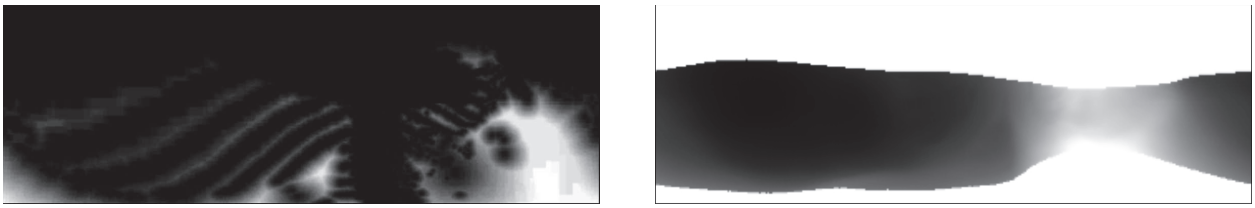

(a) (b)

Figure 3. Examples of constraint maps generated using volume rendering. (a): The *risk structure distance* constraint map. (b): The *penetration depth* constraint map.

Liver capsule penetration angle: We modified the volume renderer using a custom shader to compute the angle between the normal vector of the liver surface and the direction of the trajectory. The normal vector is computed based on a resampled and smoothed liver mask, because gradient estimation for binary images as well as strong anisotropic voxels can be problematic. This modification of the input liver mask can be integrated into a preprocessing step.

Tumor coverage: We use a simple approximation to determine the coverage of the tumor volume for all trajectories based on the following observations:

- Those trajectories close to the main tumor axis facilitate a good coverage of the tumor volume for applicators with longish ablation areas such as needle-shaped applicators (Figure 4(b)).
- For applicators with an ablation area of flat shape (umbrella-shaped applicators), those trajectories are preferred too, because they permit coverage of the tumor by pulling the applicator back along the trajectory (Figure 4(c)).

Therefore, we encode the deviation to the main tumor axis for each trajectory. Volume rendering is not required for this constraint map. Instead, we use simple image processing steps to compute the deviation for each trajectory. In the first step, we compute the spherical coordinates of the two trajectories that are parallel to the tumor axis (Figure 4(a)). These coordinates are used as centers of two radial distance fields. Both fields are combined using a minimum operator and stored into the map (Figure 4(d)). A special border handling ensures that parts of the distance fields beyond 360° or 0° of longitude are shifted adequately. Because the image domain is a 2D spherical coordinate system, the resulting pixel values of the map are the deviations from the main tumor axis in degrees. This constraint is only used for tumors of a considerably elongated shape.

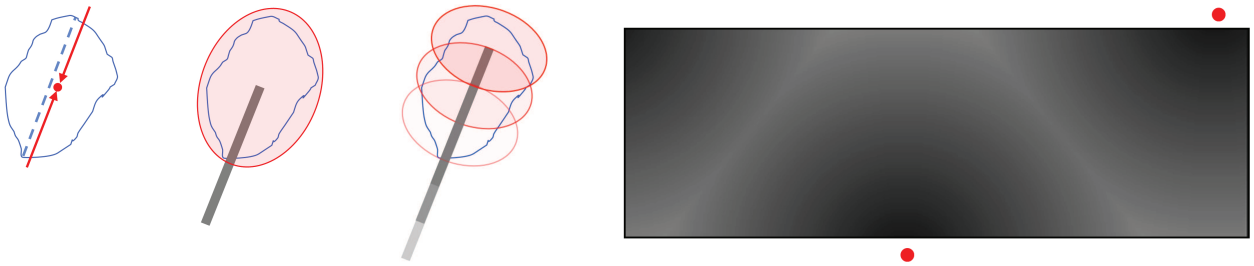

(a) (b) (c) (d)

Figure 4. The computation of the tumor coverage constraint is based on the analysis of the main tumor axis. (a): There are two trajectories *(red arrows)* that lie parallel to the main tumor axis *(dashed line)*. (b): Coverage of the tumor with one longish ablation area. (c): Coverage of the tumor volume with multiple ablations on the trajectory. (d): The resulting constraint map for the computed main tumor axis. The two trajectories that are parallel to the axis *(red points)* are outside the range of -60° to 60° in this example.

Angulation: The angulation to the transversal plane corresponds to the latitudinal angle. Therefore, we generate a map that stores the respective latitude value in each pixel. All pixels of one row have the same value, because the respective trajectories have the same latitude. Because angulation from cranial to caudal might be treated differently than angulation from caudal to cranial, we store the signed values. Therefore, the values range from -60° to 60° where negative values represent angulations from caudal to cranial.

Circumference This map simply stores the longitudinal angle of each trajectory. Similar to the previous constraint map, we can generate the map generically, because the longitude of a trajectory corresponds to the column of the respective pixel. The values range from 0° to 359°.

4.2 Rating of constraint maps

The seven constraint maps $\boldsymbol{M}_i$ contain values for each possible trajectory in adequate units and value ranges. However, this does not express any rating of the respective values. Therefore, we apply a rating function $\boldsymbol{f}_i$ to each map to penalize unwanted and to favor wanted characteristics. Each of these functions assigns values between 0 and 1 to each constraint value, whereas low values indicate unwanted and high values favored characteristics. As an example, Figure 5 illustrates the rating for the *angulation* constraint map $\boldsymbol{M}_a$. The unrated map contains values from -60° to 60°. The function $\boldsymbol{f}_a$ assigns values between 0 and 1. The peak of the function is at 0 in order to favor trajectories that are in plane. Negative values of $\boldsymbol{M}_a$ correspond to angulations from caudal to cranial and are better suited than angulations from cranial to caudal. Hence, the function is not symmetrical. The rating of the *circumference* constraint differs from the other constraints in that three rating functions are used. This is necessary because different restrictions apply depending on the position of the target. Based on the location of the target point with respect to the four quadrants in the transversal plane, the respective function is chosen (see Figure 6).

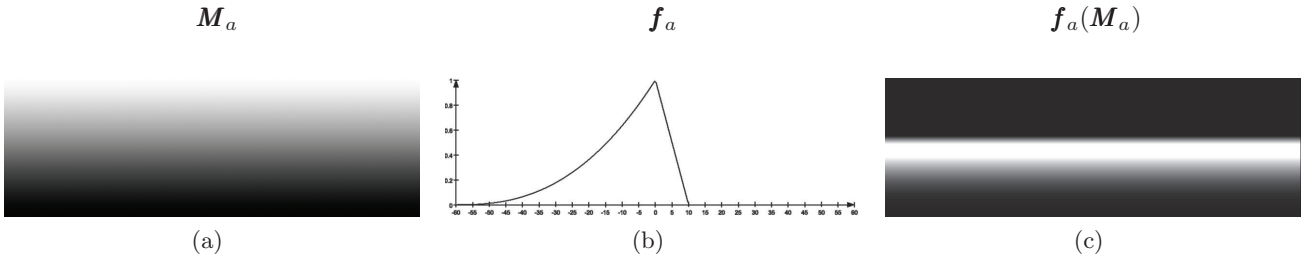

Figure 5. Rating of the *angulation* constraint map. (a): The unrated map contains values from -60° *(bottom)* to 60° *(top)*. (b): The asymmetrical rating function assigns values between 0 and 1. (c): The rated constraint map favors trajectories close to the transversal plane and penalizes trajectories from cranial to caudal more than trajectories from caudal to cranial.

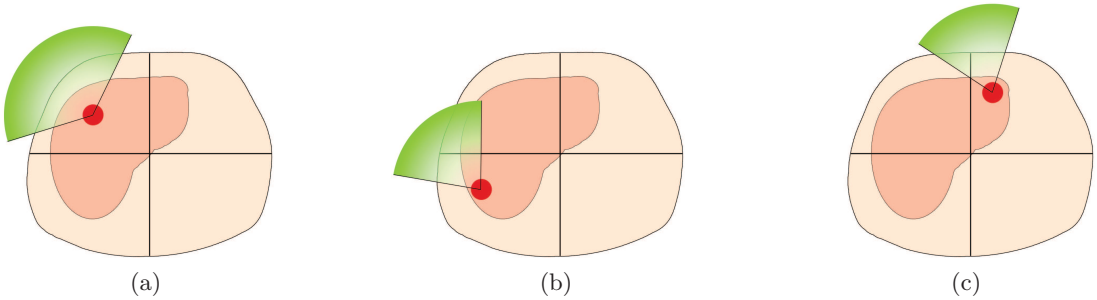

Figure 6. Rating of the *circumference* constraint map: Different restrictions apply to the posterior right (a), the anterior right (b) and posterior left (c) part of the liver.

4.3 Combination of constraint maps

After rating, the maps are combined in one single image. We do not use a weighted sum in order to prevent a situation in which good values of one constraint compensate poor values of other constraints. Instead, we compute the combined map $\boldsymbol{M}_c$ by multiplication of the weighted maps:

$$\boldsymbol{M}_c = \prod_i (\boldsymbol{f}_i(\boldsymbol{M}_i) * \boldsymbol{w}_i + 1 - \boldsymbol{w}_i)$$

where $\boldsymbol{w}_i$ denote the respective weighting factors. A weighting factor of 0 results in no influence of the corresponding constraint, while 1 results in full influence. This weighted product also ensures that trajectories are excluded which have a value of 0 for a constraint with a weighting factor of 1. Hence, such constraints can be considered *strict* constraints. The normalization term $1 - \boldsymbol{w}_i$ is needed because the product would be 0 if one of the weighting factors was 0. The values of $\boldsymbol{M}_c$ are in the range of 0 to 1.

4.4 Extraction of suited paths

To compute the maxima of $\boldsymbol{M}_c$ we apply a Gaussian smoothing and thereafter determine for each voxel whether it is a local maximum inside a 3x3 neighborhood. We extract all maxima, store their respective longitude and latitude values, and sort them based on their value in $\boldsymbol{M}_c$. The maximum with the highest value is automatically selected, but any other maximum may be chosen by the user. An overview of the complete algorithm is given in Figure 7.

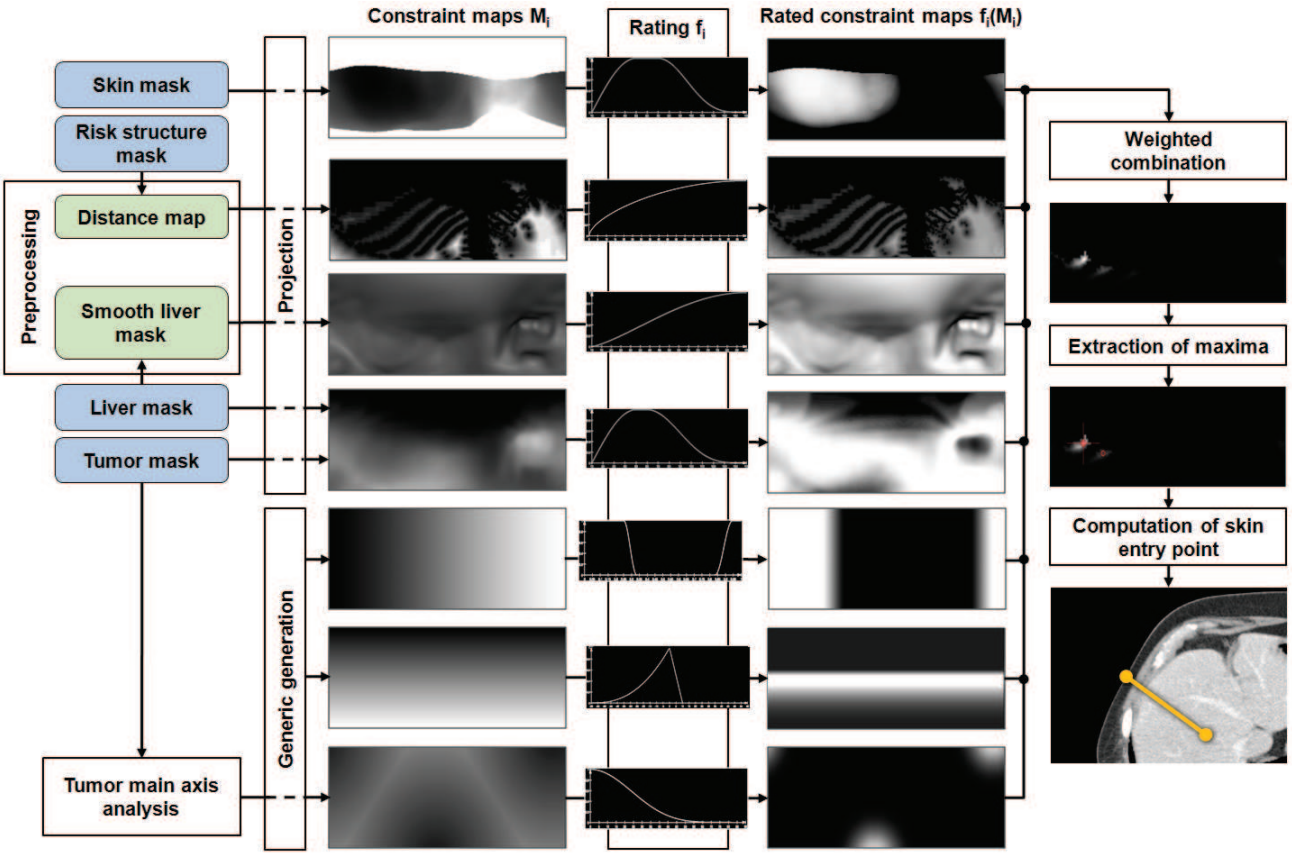

Figure 7. Outline of our algorithm: Constraint maps are generated based on the input masks (blue) and preprocessing results (green) (from top to bottom: *penetration depth, distances to risk structures, liver capsule penetration angle, portion of healthy liver tissue, circumference, angulation, tumor coverage*). After rating, they are combined into one image from which maxima are extracted.

For the purpose of visualization, the skin entry point for the selected proposal might be needed. This can be computed based on the target position, the longitude and latitude values of the trajectory, and the corresponding penetration depth, which can be looked up in the penetration depth map. The resulting path can be visualized by drawing a line or a virtual applicator model.

5. RESULTS

We implemented the proposed method with focus on CT guided RFA and biopsy using the rapid prototyping platform MeVisLab[17] and integrated it into a clinical prototype. The preprocessing step, which contains the computation of the risk structures distance transformation and the resampled smooth liver mask, is carried out automatically after segmentation of the liver, skin, and risk structures. Its mean duration is 4 seconds for abdominal scans of moderate size (512 x 512 voxels per slice, 44 - 203 slices) on a standard laptop computer (Intel Core2 Duo T9500 @ 2,6 GHz, 3 GB Ram, NVIDIA GeForce 8600M GT, Windows Vista 32Bit). Once the physician has segmented the tumor, trajectory proposals for the tumor center are generated in less than 1 second. The best proposal is automatically visualized by means of a virtual applicator. The physician can move the tip of the virtual applicator, if necessary, and the proposals are updated as soon as the interaction is finished. Again, this is executed in less than 1 second. After each update, the physician can step through the list of proposals.

During several workshops with radiological experts, we successively discussed and refined the aforementioned constraint maps and the respective rating functions and weighting factors. Based on this expert knowledge, we adjusted the algorithm and its parameters in an iterative process. To verify the suitability of the chosen rating functions and weighting factors, we conducted an additional investigation of the path parameters of actually placed applicators. The study covered 37 different RF access paths defined by three radiologists on 19 different RFA CT planning scans (not each radiologist performed the planning for all images). After manually deriving the path parameters for each access path, we calculated the average value as well as the upper and lower bound for each parameter. We then compared these values with the previously defined rating functions and adjusted them when necessary. Although the algorithm parameters have been determined with focus on RFA, they are also appropriate for biopsy planning, because except for tumor coverage, the radiologists consider the same criteria during planning.

In a preliminary informal evaluation, we applied the method to several RFA CT planning scans. We compared the proposals that were generated by our method with the respective peri-interventional scans, which included the actually placed needle, or discussed the results with our clinical partners. In all cases, the proposal list contained the path that was actually chosen for the intervention, or to the path the physician would have chosen. Furthermore, in most cases, the first proposal of the list corresponded to that path. Small deviations of the trajectory could be observed, but in all cases, the chosen intercostal space matched the choice of the expert (Figure 8).

At present, we are conducting a study which investigates the clinical relevance of our method for the planning of radiofrequency ablation. The used implementation does not include the tumor coverage constraint yet. For 25 RFA CT planning scans, an expert radiologist evaluates the three best access path proposals generated by our algorithm and compares them to the access paths that were planned in advance by three experienced radiologists. First results show that all proposals offered by our method are technically feasible. More precisely, most of them are very good. With a rating range of 1 - 6 (1 = very good, 6 = not suitable), 63 of 75 proposals were graded 1 or 2. The average rating of all proposals is 1.77. Most of the cases that were rated worse than 1 suffered from the same problem: The recessus was penetrated by the generated path. The algorithm could not take the recessus into account, because it was not included in the segmentation masks.

In another clinical study, which will start shortly, we will consider path planning for liver biopsy. Two experts will define the best possible access path and then compare this gold standard to the three best automatically generated access paths.

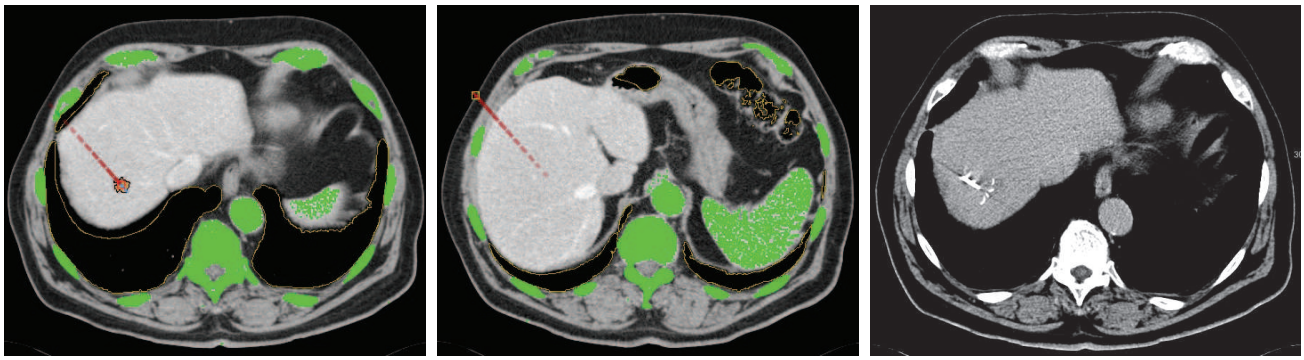

(a) (b) (c)

Figure 8. Example of a path proposal (red) for a lesion beneath the liver dome (visible in Figure (a), orange, black outline): the trajectory is double oblique, the skin entry point (Figure (b)) is in another slice than the target point (Figure (a)). Segmentation masks for high density (green) and low density (yellow outline) risk structures are visualized as overlays. Figure (c) shows one slice of the peri-interventional scan with the actually placed needle for comparison.

6. CONCLUSION

In this work, we presented a method that automatically generates access path proposals for hepatic needle placement considering multiple clinically relevant criteria. It uses segmentation masks of the skin, liver, tumor, and risk structures as input. Polygonal representations of theses structures are not required. Thus, our method can be easily integrated into existing planning software assistants. The application of techniques from the fields of computer graphics and image processing as well as the utilization of the graphics hardware facilitate very low computation times. After choosing a target point, the computation is carried out in less than 1 second, and the physician can immediately examine the proposed access paths. Additionally, interactive updates upon changes of the target point position or other parameters, such as constraint weights, are feasible. Therefore, our method is suited to enhance the planning process without adding considerable computational overhead. First results of the ongoing evaluation process show that our method generates path proposals that are suited to support the planning of radiofrequency ablation and biopsy.

The adaptation of the method to other percutaneous interventions will be investigated in the future. Although the radiofrequency ablation of larger tumors is still rather rare, we will also investigate the adaptation of our method for that scenario, because it requires a considerably higher amount of planning. For this purpose, we plan to incorporate solutions for the volume coverage problem.

ACKNOWLEDGMENTS

This work was funded by Siemens AG Healthcare Sector Imaging & IT Division Computed Tomography, Forchheim. We would like to thank our colleagues at Fraunhofer MEVIS for their contribution to our work.

REFERENCES

[1] Mahnken, A. H. and Ricke, J., eds., [*CT- and MR-Guided Interventions in Radiology*], Springer (2009).

[2] Garrean, S., Hering, J., Saied, A., Helton, W. S., and Espat, N. J., "Radiofrequency ablation of primary and metastatic liver tumors: a critical review of the literature," *Am J Surg* **195**(4), 508–520 (2008).

[3] Butz, T., Warfield, S. K., Tuncali, K., Silverman, S. G., Sonnenberg, E. v., Jolesz, F. A., and Kikinis, R., "Pre- and intra-operative planning and simulation of percutaneous tumor ablation," *Proceedings of MICCAI*, 317–326 (2000).

[4] Powell, M. J. D., "An efficient method for finding the minimum of a function of several variables without calculating derivatives," *The Computer Journal* **7**(2), 155–162 (1964).

[5] Villard, C., Soler, L., Gangi, A., Mutter, D., and Marescaux, J., "Towards realistic radiofrequency ablation of hepatic tumors 3d simulation and planning," *Proceedings of SPIE* **5267**, 586–595 (2004).

[6] Zhang, H., Banovac, F., Munuoc, S., Campos-Nanezc, E., Abeledoc, H., and Cleary, K., "Treatment planning and image guidance for radiofrequency ablation of liver tumors," *Proceedings of the SPIE* **6509**, 650922.1 – 650922.10 (2007).

[7] Mundeleer, L., Wikler, D., Leloup, T., Lucidi, V., Donckier, V., and Warzée, N., "Computer-assisted needle positioning for liver tumour radiofrequency ablation (rfa)," *Int J Med Robot* **5**(4), 458–464 (2009).

[8] Trovato, K., Dalal, S., Krücker, J., Venkatesan, A., and Wood, B. J., "Automated rfa planning for complete coverage of large tumors," *Proceedings of the SPIE* **7261**, 72610D.1–72610D.7 (2009).

[9] Altrogge, I., Preusser, T., Kröger, T., Büskens, C., Pereira, P. L., Schmidt, D., and Peitgen, H.-O., "Multi-scale optimization of the probe placement for radiofrequency ablation," *Academic Radiology* **14**(11), 1310–1324 (2007).

[10] Chen, C.-C. R., Miga, M. I., and Robert L. Galloway, J., "Optimizing electrode placement using finite-element models in radiofrequency ablation treatment planning," *IEEE Transactions on Biomedical Engineering* **56**(2), 237–245 (2009).

[11] Baegert, C., Villard, C., Schreck, P., and Soler, L., "Multi-criteria trajectory planning for hepatic radiofrequency ablation," *Proceedings of MICCAI* **4792**, 676–684 (2007).

[12] Baegert, C., Villard, C., Schreck, P., and Soler, L., "Precise determination of regions of interest for hepatic rfa planning," *Proceedings of the SPIE* **6509**, 650923.1–650923.8 (2007).

[13] Williams, L., "Casting curved shadows on curved surfaces," *SIGGRAPH Comput. Graph.* **12**(3), 270–274 (1978).

[14] Chan, M.-Y., Qu, H., Wu, Y., and Zhou, H., "Viewpoint selection for angiographic volume," *ISVC*, 528–537 (2006).

[15] Mühler, K., Neugebauer, M., Tietjen, C., and Preim, B., "Viewpoint selection for intervention planning," *Proceedings EuroVis*, 267–274 (2007).

[16] Baegert, C., Villard, C., Schreck, P., Soler, L., and Gangi, A., "Trajectory optimization for the planning of percutaneous radiofrequency ablation of hepatic tumors," *Comput Aided Surg* **12**(2), 82–90 (2007).

[17] Bitter, I., Van Uitert, R., Wolf, I., Ibanez, L., and Kuhnigk, J.-M., "Comparison of four freely available frameworks for image processing and visualization that use itk," *IEEE Transactions on Visualization and Computer Graphics* **13**(3), 483–493 (2007).